B0812

Thermal effects on polarisation curve in high compacitness CEA stack

Stephane Di Iorio, Thomas Carlioz, Manon Elie
Univ. Grenoble Alpes, CEA, Liten, DTCH, 38000 Grenoble, France
Tel.: +33-478383429
stephane.diiorio@cea.frj

The interest in high-temperature electrolysis technology persists due to its potential for cost-effective and low-carbon hydrogen production. To facilitate the deployment of pre-industrial systems, CEA is dedicating considerable resources to scaling up its proprietary stack-based design and gaining deeper insights into optimizing its utilization.
A 25-cell CEA stack with a 100 cm² active area is under examination. A notable characteristic of the CEA stack is its exceptional compactness, standing at a height of 62 mm, inclusive of two end plates each measuring 20 mm. This compact configuration, combined with the heat generated or consumed by electrochemical reactions and electrical currents, results in significant thermal effects.
An experimental investigation is underway to explore these effects during hydrogen production. Initially, a series of polarization curves is recorded at intervals of 10°C between 700 and 800°C, employing a rapid ramp-up of current. Subsequently, stabilized operational points are recorded at various furnace temperatures, spanning a current range from 0 to 1.85 A/cm². A substantial discrepancy in average cell voltage is observed depending on the mode of operation: either a rapid current ramp-up or a gradual increase with extended stabilization periods. This difference is primarily attributable to thermal effects.
While temperatures are monitored using peripheral thermocouple probes at each stabilized operating point, an innovative method has been successfully employed to gather internal temperature data within the stack. Despite the presence of high thermal vertical gradients, no mechanical damage has been detected.

Introduction

The European Commission has unveiled its roadmap towards achieving a competitive low-carbon economy by 2050. To realize this vision of the European "Green Deal," a fundamental rethinking of clean energy supply policies across all economic sectors is imperative [1]. Hydrogen emerges as a pivotal player, serving as a resource for industrial processes, a transportation fuel, and a medium for high-capacity and long-distance electricity storage [2]. Anticipated is a substantial rise in hydrogen's share within the broader European energy mix, projected to reach 13-14% by 2050, compared to the current less than 2% [3].

In light of this trajectory, there arises a pressing need to augment the production capacity of carbon-free hydrogen, primarily through water electrolysis. At the European level, a deployment plan targeting 100 GW of electrolysis by 2030 has been proposed [2], aiming to yield an annual production of 10 million tons of hydrogen during its operational phase, alongside an additional 100 GW allocated for export.

Furthermore, the current cost competitiveness of carbon-free hydrogen production vis-à-vis conventional methods utilizing fossil fuels, notably methane steam reforming, remains a challenge. The deployment of high-power electrolyzers holds promise in substantially reducing the cost of low-carbon hydrogen production. Additionally, electrolysis presents significant potential for innovation, offering avenues to enhance performance, longevity, and efficiency—crucial parameters influencing hydrogen's cost [4-5].

Among various electrolysis technologies, Solid Oxide Electrolysis (SOE) stands out for its superior efficiency, positioning it as a highly promising avenue for low-cost hydrogen production. Forecasts predict a levelized cost of hydrogen as low as 2 €/kg for electrolysis plants operating at a scale of hundreds of MW, with an electricity cost of 40 €/MWh [6].

1 Experimental

1.1 Cells

The cells considered for the present works were commercial fuel electrode supported cells from Elcogen. They consist of ~380 µm Ni/3YSZ support layer, a ~5 µm Ni fuel contact layer, a ~12 µm Ni/8YSZ fuel active layer, a ~7 µm thick LSC (Lanthanum–Strontium Cobaltite) oxygen electrode, a ~2µm 8YSZ (8mol% yttria stabilized zirconia) electrolyte and a CGO (Gadolinia doped Ceria) barrier layer of similar thickness. Square cells of 120 x 120 mm are used, and an active area of 100 cm²

1.2 Stacks

The stack design considered, as already presented in [7] was based on thin interconnects using AISI441 ferritic stainless steel sheets. A nickel-mesh and an LSM (Lathanum-Strontium Manganite) contact element were set between the cell and the interconnect in the H2 and O2 compartments respectively. A cross flow design was chosen. Sealing was achieved with a commercial ceramic glass. A mica foil was added to ensure the electrical insulation between two adjacent interconnects, but also to complete the sealing and to precisely position the cell.

The presented stack are made of 25 cells with an active area of 100 cm². The stack, extensively described in [8] and assembled in a reliable way with initial performances with a very low scattering [9] and ability to be scale up [10], is taken as a reference for the developments performed in the present study.

A particularity of CEA stack is its high compactness with a height of 62 mm including 2 end plates of 20 mm. Such compactness coupled with heat production or consumption due to electrochemical reaction and electrical current lead to high thermal effects.

1.3 Experimental setup and testing conditions

A in-house developed test bench was used to test the stack. To optimize the sealing and the electrical contact, a mechanical loading of 2 kN was applied to the stack by external system.
Thermocouples (N-type) were located in holes drilled in the thick endplates (4 up and 4 down) of the stacks and in endplates and in the gas flow. Accuracy at test temperature is ±3°C.
Current was applied with the help of EA-PSI 8080-340 power supply and with two current rods fixed to the stack endplates. Voltage probes were spot-welded to each interconnect to measure the voltage of each cell.
The stack gas connections to the test bench were done through an in-house developed solution based on a form of a high temperature gas manifold.
Current and stack voltage were recorded as well as individual cell voltages. Bronkhorst mass flow-controllers adjusted the gas supply and mass flow meters were set at the outlet of each compartment, after condensation of the unused water in case of the hydrogen side, in order to evaluate the stack gas tightness at Open Cell Voltage (OCV) or under polarization. Accuracy of the multiple instrumentation systems that equip the benches is in the same order of magnitude. Main measurement accuracy specifications are the following: current ± 1%, total stack voltage ± 1%, i-V pressures ±2mbar, mass flows ±3%.
The testing procedure started by heating the stack for sealing and reduction. Following reduction, the stacks underwent an initial stabilization period of 500 hours. The total flow rate was set at 18 Nml/min/cm², comprising 90% H2O and 10% H2. Air flow was regulated to maintain a 30 mbars overpressure on the air side compared to the H2 side.
Subsequent to stabilization, the Area Specific Resistance (ASR) was characterized using polarization curves (referred to as i-V curves) between 700°C and 800°C after a 2-hour stabilization period. The current ramp rate was set at 150 A/min to minimize thermal effects on the stack. ASR measurements were taken between 0.95 and 1.1 V to ensure they remained within the linear portion of the curve. Under these conditions, the furnace temperature closely matched the measured end plate temperature, with a deviation of approximately ±1°C. Stabilized current points were established at a furnace temperature of 750°C, ranging from 0 to 185 A (1.85 A/cm²) with increments of 5 or 10 A.
Over 40 i-V curves were generated before and after the stabilized curve, spaced apart by 300 hours. Measurements were conducted within temperature ranges of 750°C to 780°C, 780°C to 730°C, 730°C to 800°C, and 800°C to 700°C. No hysteresis behavior was observed, even before and after the stabilized i-V curve. Initial (500 hours) and final (800 hours) curves exhibited similarity, indicating negligible degradation of the stack during the test.
Endplates temperatures were measured in the upper and lower thick end plates (20 mm) using four thermocouples inserted into thin holes in the middle thickness of each plate. Consequently, the end plate temperature represents the average of eight thermocouples.

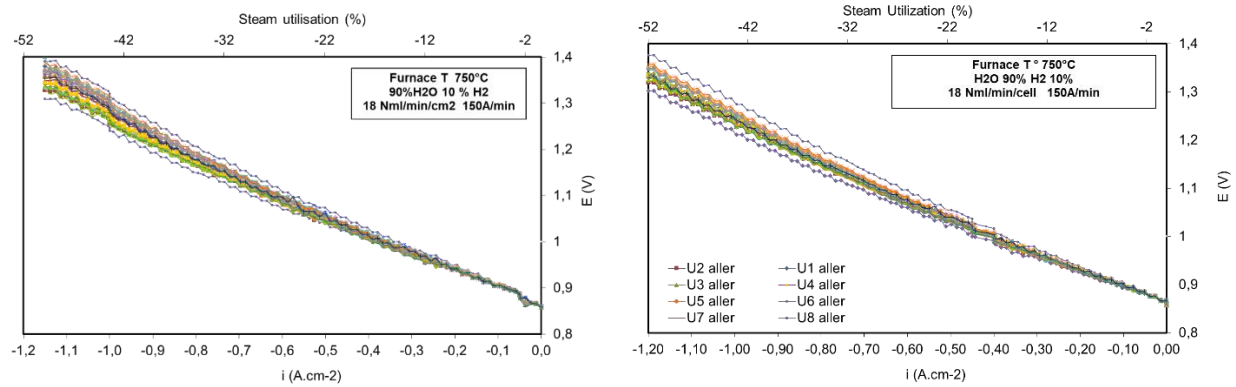

Figure 1: i-V curves in SOE mode at 750°C for 25 cells stack. Total flow rate of 12 NmL min-1 cm-2 of 90/10 vol.% H2O/H2 mix is provided to the fuel electrode, air on the other side. Steam conversion is reported by secondary abscissa axis on top of the graph. Curve recorded a) 500 h after the test beginning b) 800 h after the test beginning.

2 Results

2.1 ASR evolution with temperature

The Area Specific Resistance (ASR) exhibits a linear evolution ranging from -0.52 Ohm.cm² at 700°C to -0.25 Ohm.cm² at 800°C (see fig 2). The experimental variation for the same temperature is approximately 0.025 Ohm.cm². A linear approximation of ASR is as follows:

$$ASR(Ohm.cm^2) = 0.0028\ T°(C) - 2.4753$$

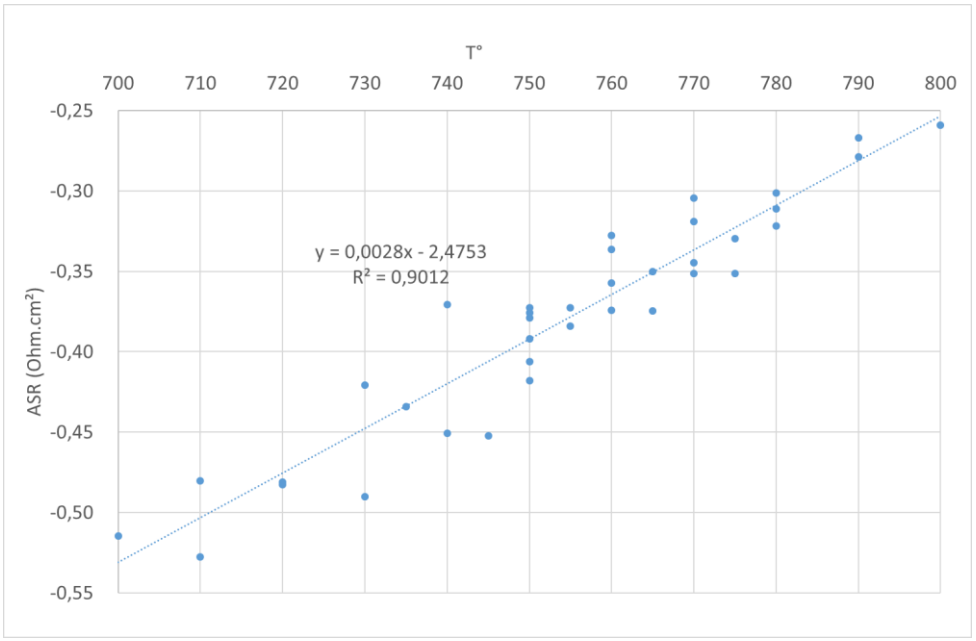

Figure 2: The ASR values are plotted against temperature, calculated within the voltage range of 0.95 V and 1.1 V.

2.2 Stabilised i-V curve

The stabilized curve obtained from stabilized current points exhibits clear differences from the polarization curve at 750°C and 150 A/min (see fig 3). The apparent stack performances for a rapid solicitation are superior up to 1.1 A/cm² compared to the stabilized condition.

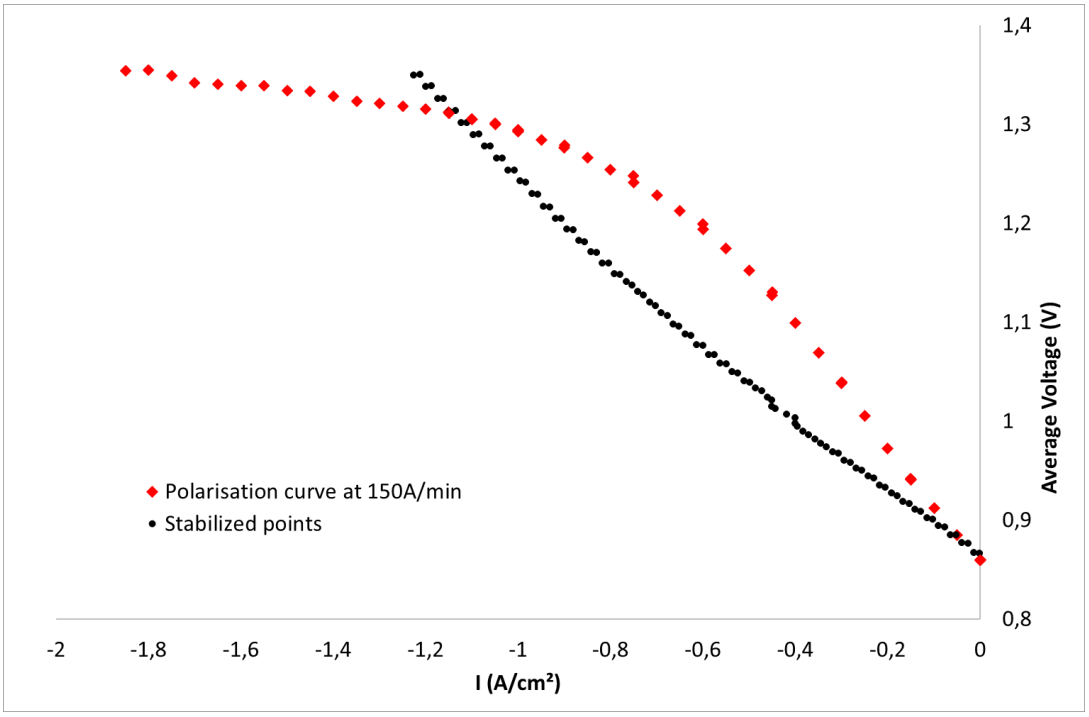

Fig. 3 : SOEC stack polarization curves with a furnace temperature of 750 °C depending of solicitation times.

During an i-V curve at 150A/min, the end plates remain close to the furnace temperature of 750°C. Conversely, for stabilized points, the stack end plate temperatures fluctuate between 738°C and 780°C (see fig. 4). It's likely that the minimal and maximal internal stack temperatures are respectively lower and higher, especially for central cells. The peak endothermic point on the stabilized curve occurs at approximately 30% (0.4 A/cm²) of the current obtained (1.2 A/cm²) at the thermoneutral voltage (1.285V) observed in the rapid i-V curve.

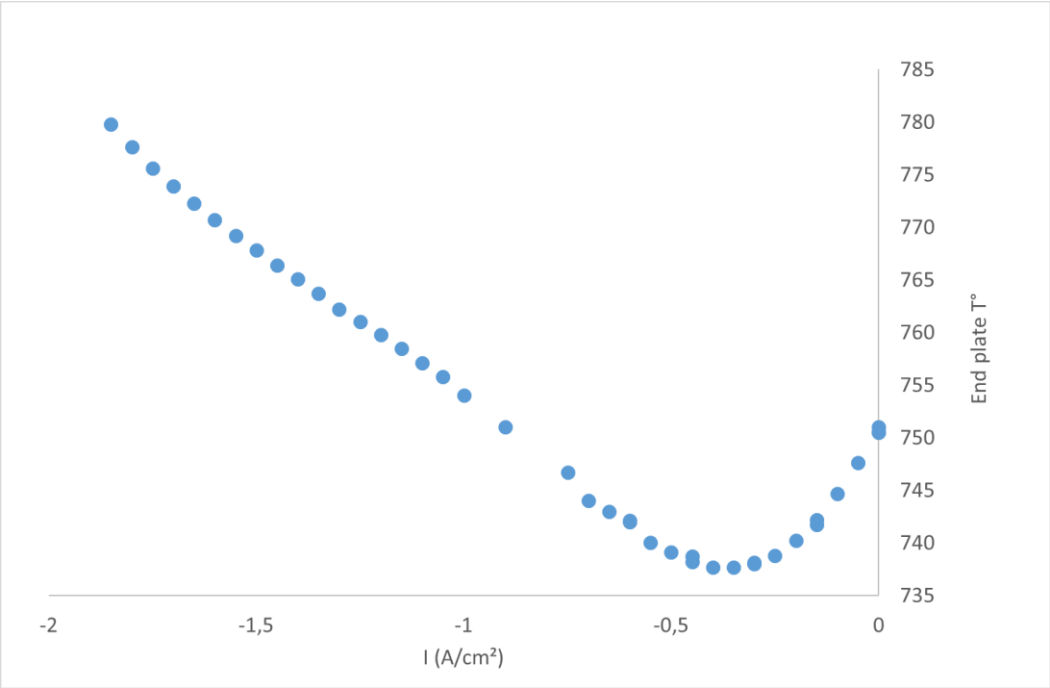

Fig 4: End plates temperature during stabilized i-V curve. The furnace t° is maintained at 750 °C

The significant disparity between the i-V curve at 150 A/min and the stabilized i-V curve can be attributed to thermal effects. The high compactness of the 25-100 CEA stack results in inefficient heat dissipation, leading to substantial temperature fluctuations caused by the heat generated or consumed by the electrochemistry.

2.3 OCV measurements

Following the stabilization at 1.85 A/cm², the current is switched off to 0 A. Upon quick measurement, the Open Circuit Voltage (OCV) for each cell reveals significant inhomogeneity between central and border cells (see fig. 5). Central cells display an OCV value of 0.82 V, while border cells exhibit 0.85 V. However, after a few minutes, all cells converge to the same OCV value. These initial discrepancies serve as evidence of thermal inhomogeneity among the stack cells. Cells 1 and 25 register an OCV of 0.84 V, characteristic of a 90/10 H2O/H2 mix at 800 °C, a temperature close to the 780 °C measured on the stack's end plates.

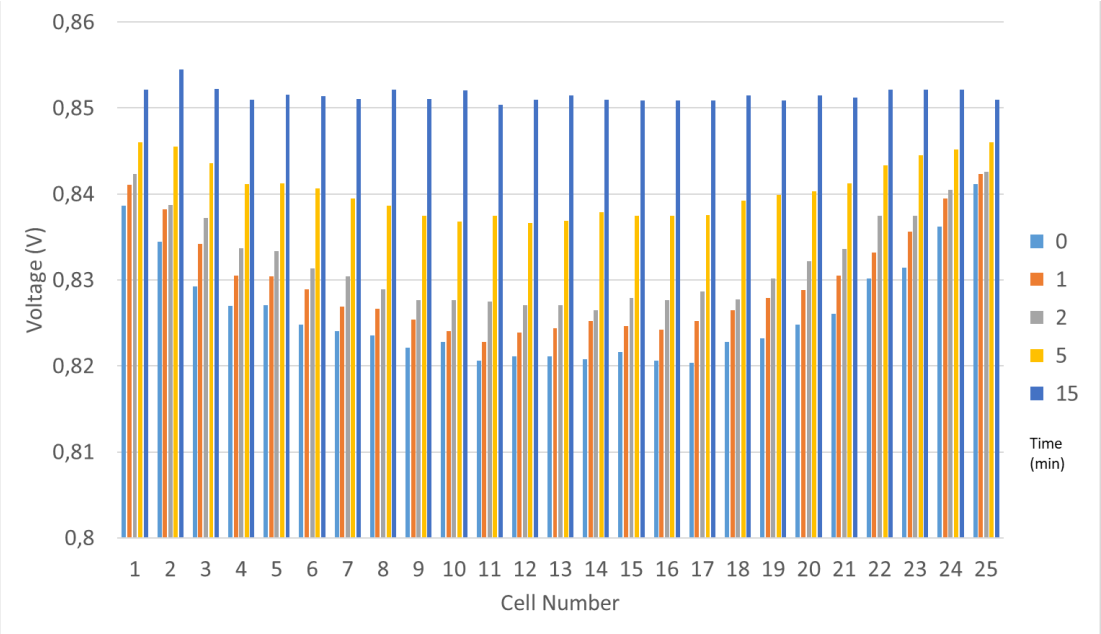

Fig 5: The stack was stabilized at 1.85 A/cm² for several hours, after which the current was abruptly cut. Open Circuit Voltage (OCV) measurements were taken within 0 to 15 minutes after the current was reduced to zero.

2.4 First simulations

For a stabilized point denoted as "1," it is feasible to compute an average $ASR_{\text{-calc-stab1}}$ of the stack using the following formula:

$$ASR_{\text{-calc-stab 1}} = (U1at\ _{\text{i-stab1}}\text{-}0.86)/i_{\text{-stab1}}$$

The $ASR_{\text{-calc-stab1}}$ is depicted in figure 6. The value decreases between 0 and -0.4 A/cm² and increases between -0.4 to -1.85 A/cm². The minimum value is -0.6 Ohm/cm² and the maximum one is -0.25 Ohm/cm².

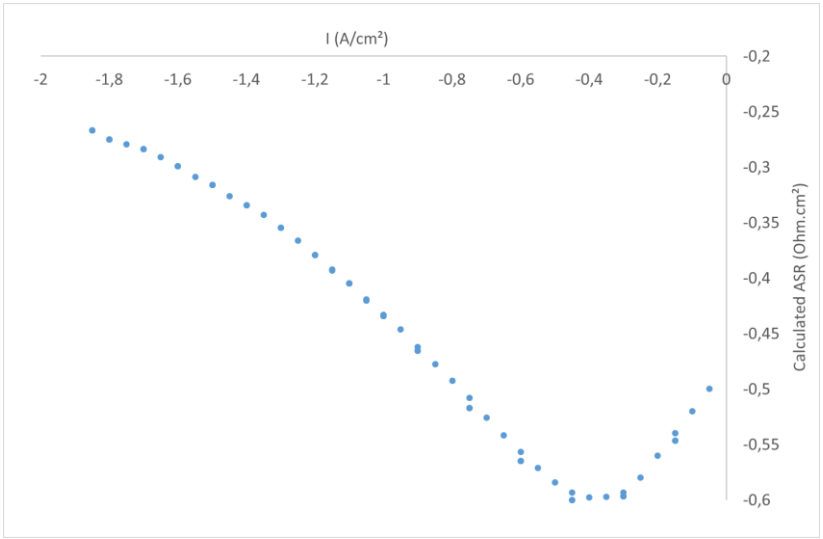

Fig 6: ASR-calc-stab calculated from stabilized points of i-V curve

From the ASR variation with temperature measured on high-speed IV curves as presented in section 3.1, it becomes possible to establish a relationship between stack temperature and the $ASR_{-calc-stab}$. This relationship enables the calculation of an average temperature for the stack.
The figure 7 compares the measured end plate temperatures with the calculated average stack temperature. A notable difference is evident between the temperatures; however, the end plate temperature clearly underestimates the average stack temperature due to easy heat exchange with furnace. The calculated average stack temperature fluctuates by approximately 115 °C during the stabilized i-V curves, with a maximum value of 789 °C observed at -1.85 A/cm² and a minimum of 670 °C at -0.4 A/cm².

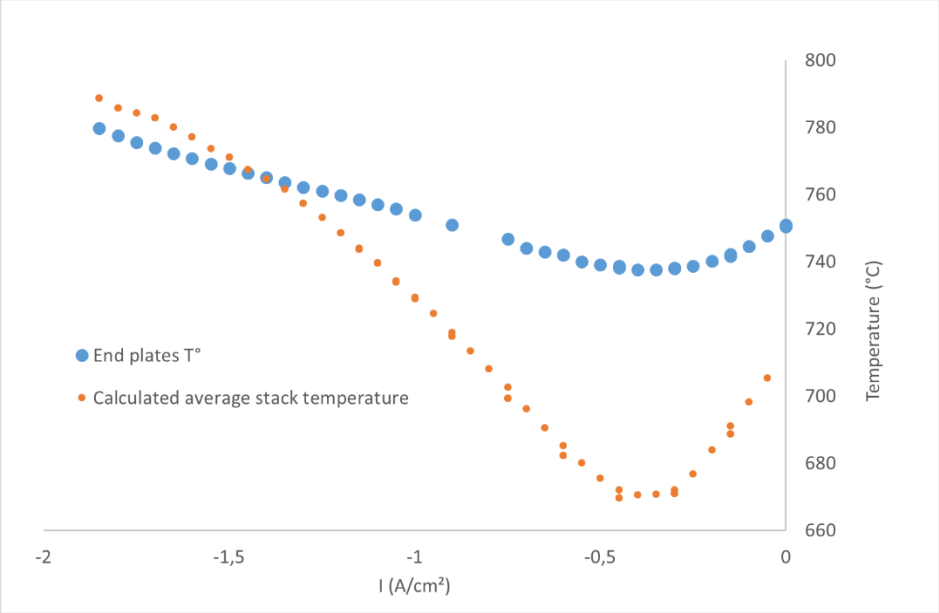

Fig. 7 : Measured end plates temperature and calculated average stack temperature

Using the Open Circuit Voltage (OCV) measured just after the current switch-off (1.85 A/cm² => 0 A/cm²) as presented in figure 5, it is feasible to derive a calculated cell temperature with the assistance of the Nernst equation (figure 8). The temperatures of the central cells (11 to 18) of the stack are calculated at 840 °C, while the external cells (1 and 25) are approximately 800°C. Thus, a z-axis gradient of about 40°C is observed. The average stack temperature calculated from the average of the 25 cells' values is 831 °C.

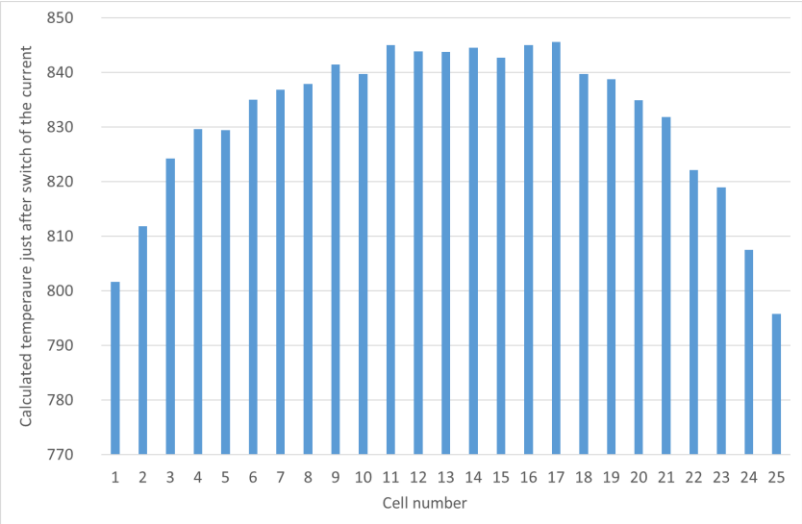

Fig 8 : Calculated temperature from OCV and Nernst law

We can observe differences between the average calculated temperature derived from the calculation based on stack ASR at 1.85 A/cm² (789°C) and that obtained from OCV (831°C).

3 Discussion

The experimental findings presented herein clearly demonstrate significant thermal effects on 25-cell and 100 cm² active area CEA stacks. Rapid i-V curves conducted at 750°C exhibit fundamental distinctions from stabilized i-V curves. Several factors account for these disparities.

Firstly, stack performance is markedly influenced by temperature, as evidenced by the apparent decrease in ASR (Area Specific Resistance) measured between 800 and 700°C, registering at half the value for the lower temperature range. Furthermore, the dense configuration of CEA stacks results in approximately a 50°C fluctuation during stabilized i-V curve measurements on the stack's end plates.

It is noteworthy that the significant thermal gradient measured did not result in any damage to the stack or compromise its performance.

These experiments yield valuable data that can inform various simulations. Initial calculations, rooted in ASR analysis, reveal an internal temperature fluctuation exceeding 110°C, with a maximum average stack temperature of 789°C recorded for a furnace temperature of 750°C. This maximum temperature closely aligns with the one measured on the end plates under the highest tested current. Conversely, the minimum calculated average stack temperature of 670°C starkly contrasts with the minimal value of 738°C observed on the end plates.

Temperature calculations based on Open Circuit Voltage (OCV) reveal substantial variances between cells situated in the middle of the stack and those on the outer periphery, amounting to approximately 40°C. Interestingly, despite this discrepancy, the calculated average temperature using the OCV method (845°C) surpasses that derived from the ASR method (789°C).

Furthermore, ASR calculations were performed within the voltage range of 0.95 to 1.1 V to ensure adherence to the linear portion of the i-V curves. The presented results indicate that this range corresponds to the endothermal hollow region, indicative of maximal thermal effects. It could be interesting to calculate ASR in other part of i-V curve to explore the effect on calculated temperature.

These significant disparities underscore the limitations of the rapid simulation methodology presented in this study. The ASR method employed for temperature calculation necessitates an adiabatic response from the stack during i-V curve analysis. However, it appears that a speed of 150 A/min may not be adequate to ensure such a response. Additionally, the presence of inhomogeneity’s in the cell plane has the potential to alter the thermal mapping of the stack.

A more refined approach, centered on thermo-electrochemical calculations, will be detailed in a forthcoming publication. This approach will be tailored using the same experimental dataset. Furthermore, results obtained from a 25-cell and 200 cm² active area stack will be included in the upcoming presentation.

Acknowledgements

We would like to thank GENVIA for financial funding for this project.

References

[1] The European Green Deal, European Commission, 11/12/2019
[2] Green Hydrogen for a European Green Deal: A 2x40 GW Initiati-Ve, Hydrogen Europe, 03/2020
[3] A hydrogen strategy for a climate-neutral Europe, European Commission, 08/07/2020
[4] J. Mougin, “Hydrogen production by high temperature steam electrolysis”, Chapter 8 in Compendium of Hydrogen Energy, Volume 1: Hydrogen production and purification, edited by V. Subramani, A. Basile and T.N. Veziroglu, Woodhead publishing series in Energy, Elsevier, 2015
[5] “Strategic Research and Innovation Agenda 2021 – 2027”, Clean Hydrogen Joint Undertaking, February 2022
[6] A. Odukoya, G.F. Naterer, M. Roeb, C. Mansilla, J. Mougin, B. Yu, J. Kupecki, I. Iordache, J. Milewski, “Progress of the IAHE Nuclear Hydrogen Di-Vision on international hydrogen production programs”, Int. Journal of hydrogen energy 41 (2016) 7878-78
[7] G. Cubizolles, J. Mougin, S. Di Iorio, P.Hanoux, S. Pylypko, “Stack Optimization and Testing for its Integration in a rSOC-Based Renewable Energy Storage System”, ECS Trans., 103 (1) 351-361 (2021)
[8] M. Reytier, S. Di Iorio, A. Chatroux, M. Petitjean, J. Cren, M. De Saint Jean, J. Aicart, J. Mougin, Stack performances in high temperature steam electrolysis Int. J. of Hydrogen Energy 40 (2015), pp 11370-11377)
[9] J. Mougin, S. Di Iorio, A. Chatroux, T. Donnier-Marechal, G. Palcoux, M. Petitjean, G. Roux, Development of a Solid Oxide Electrolysis Stack Able to Operate at High Steam Conversion Rate and Integration into a SOE System ECS Trans, 78 (1) 3065-3075 (2017)
[10] S. Di Iorio, T. Monnet, G. Palcoux, L. Ceruti, J. Mougin, Solid oxide electrolysis stack development and upscaling Fuel Cells 23 (6), 2023, 363-500 (2023)

Keywords: EFCF2024, Solid Oxide Technologies, SOC, Fuel Cells, SOFC, Electrolysers, SOE, thermal effects, High compactness stack